Synchronization of coupled rotators: Josephson junction ladders and the locally coupled Kuramoto model

B. C. Daniels, S. T. M. Dissanayake, and B. R. Trees*
Department of Physics and Astronomy, Ohio Wesleyan University, Delaware, Ohio 43015
(Received 9 August 2002; revised manuscript received 27 November 2002; published 26 February 2003)

We show that the resistively shunted junction (RSJ) equations describing a ladder array of overdamped, critical-current disordered Josephson junctions that are current biased along the rungs of the ladder can be mapped onto a Kuramoto model with *nearest neighbor*, sinusoidal couplings. This result is obtained by an averaging method, in which the fast dynamics of the RSJ equations are integrated out, leaving the dynamics which describe the time scale over which neighboring junctions along the rungs of the ladder phase and frequency synchronize. We quantify the degree of frequency synchronization of the rung junctions by calculating the standard deviation of their time-averaged voltages, σ_ω, and the phase synchronization is quantified by calculating the time average of the modulus of the Kuramoto order parameter, $\langle|r|\rangle$. We test the results of our averaging process by comparing the values of σ_ω and $\langle|r|\rangle$ for the original RSJ equations and our averaged equations. We find excellent agreement for dc bias currents of $I_B/\langle I_c\rangle \gtrsim 3$, where $\langle I_c\rangle$ is the average critical current of the rung junctions, and critical current disorders of up to 10%. We also study the effects of thermal noise on the synchronization properties of the overdamped ladder. Finally, we find that including the effects of junction capacitance can lead to a discontinuous synchronization transition as the strength of the coupling between neighboring junctions is smoothly varied.

DOI: 10.1103/PhysRevE.67.026216 PACS number(s): 05.45.Xt, 05.40.−a, 74.50.+r, 74.40.+k

I. INTRODUCTION

Systems of coupled limit-cycle oscillators are ubiquitous in nature, with many examples that have been studied in biology, chemistry, and physics [1,2]. One area of interest in such systems of oscillators is the synchronization of their frequencies and phases, a topic which has piqued researchers' interest for decades and continues to be a rewarding area of study in many disciplines [3]. In particular, phase models of the Winfree type [4] have been extensively studied. Winfree proposed a model in which the rate of change of each oscillator's phase in an array is dependent weakly on the difference between that particular oscillator's instantaneous phase and the phases of all the other oscillators. In one dimension, a generic version of this model for N oscillators is

$$\frac{d\theta_j}{dt} = \Omega_j + \sum_{k=1}^{N} \sigma_{j,k}\Gamma(\theta_k - \theta_j), \tag{1}$$

where θ_j is the phase of the jth oscillator and can be envisioned as a point moving around the unit circle with angular velocity $d\theta_j/dt$, Ω_j is its angular velocity or frequency in the absence of coupling to other oscillators, $\Gamma(\theta_k-\theta_j)$ is the coupling function, and $\sigma_{j,k}$ describes the range and nature (e.g., attractive or repulsive) of the coupling. The special case in which $\Gamma(\theta_k-\theta_j)=\sin(\theta_k-\theta_j)$ and $\sigma_{j,k}=\alpha/N$, where α is a constant, corresponds to the uniform, sinusoidal coupling of each oscillator to the remaining $N-1$ oscillators. This mean-field system is historically known as the (globally coupled) Kuramoto model (GKM). Kuramoto was the first to show that for this particular form of coupling and in the $N\to\infty$ limit there was a continuous dynamical phase transition at a critical value of the coupling strength α_c and that for $\alpha>\alpha_c$ phase and frequency synchronization appear in the system [5,6]. Variations on the GKM are easy to imagine. For example, if $\sigma_{j,k}=\alpha\delta_{j,k\pm1}$ while the coupling function retains the form $\Gamma(\theta_k-\theta_j)=\sin(\theta_k-\theta_j)$, we have the case where the jth oscillator is sinusoidally coupled only to its nearest neighbors in the array. Such a variation could be called the locally coupled Kuramoto model (LKM). In the case of the LKM, the lack of long range coupling means that the system is unable to yield a finite value for α_c in the $N\to\infty$ limit, a result that is true for any number of spatial dimensions [7]. As a consequence, analytic progress in understanding the conditions required for frequency and phase synchronization in the LKM is difficult to make, and most studies for which $\sigma_{j,k}=\alpha\delta_{j,k\pm1}$ involve solving Eq. (1) numerically [8–10].

Josephson junction (JJ) arrays are widely regarded as an excellent example of a physical system of coupled nonlinear oscillators. Through modern fabrication techniques and careful experimental methods, they offer a high degree of control over the parameters that drive the dynamics of the array, so that it is feasible to test specific aspects of an array's behavior [11]. Also, from an applied physics perspective, they are excellent candidates for submillimeter wave generators, which should be capable of transferring power at usable levels to a load [12–14]. Among the many different geometries of JJ arrays that have been studied, ladder arrays (see Fig. 1) deserve attention for several reasons. They exhibit rich dynamical behavior, including but not limited to time-dependent, spatially localized states, i.e., discrete breathers [15]. Their complexity is between that of better understood serial arrays and full two-dimensional (2D) arrays (e.g., square arrays). In fact, a ladder can be considered as a sub-

*Electronic address: brtrees@owu.edu

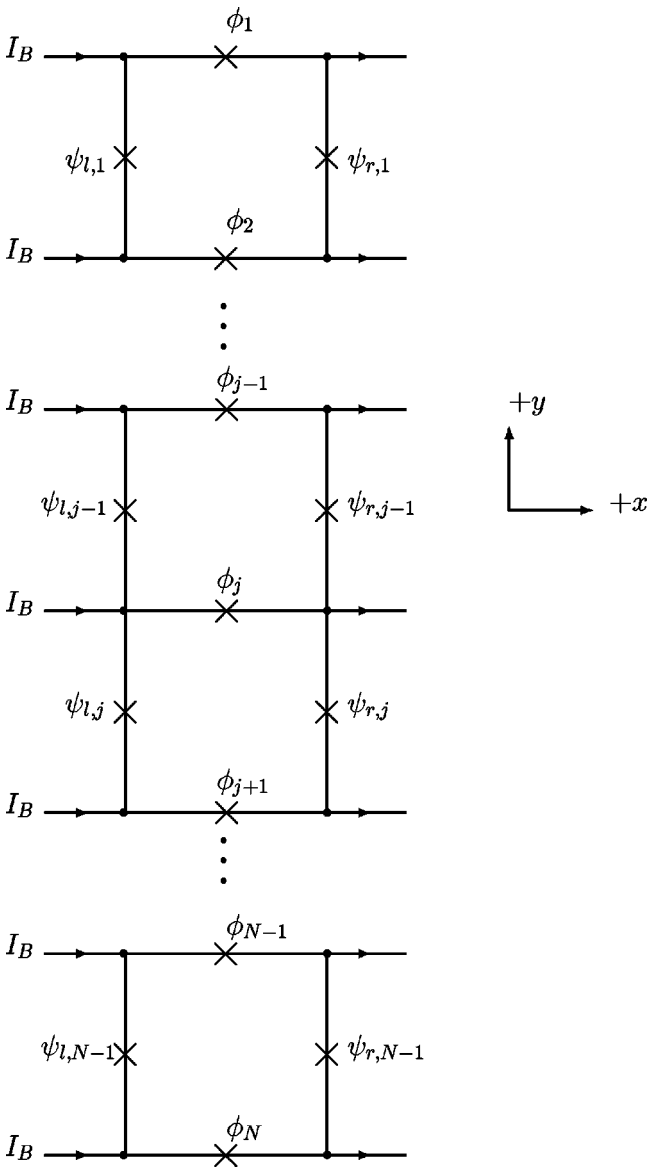

FIG. 1. A schematic of a ladder array of Josephson junctions with open boundary conditions, N horizontal junctions, and $N-1$ plaquettes. The bias current I_B is inserted at the left node of each horizontal junction and extracted from the right node. A ladder with periodic boundary conditions and $N-1$ plaquettes would result by connecting the two ends together. Then horizontal junctions labeled ''1'' and ''N'' would actually be the same junction.

unit of a square or rectangular array, and so the study of ladders could throw some light on the behavior of commonly fabricated and studied 2D arrays. Also, linearly stable phase locking of the horizontal junctions in a ladder (see Fig. 1), in the absence of a load, is observed over a wide range of dc bias currents and junction parameters, such as junction capacitance [16], so that synchronization in this geometry appears to be robust.

When a Josephson junction is biased in the voltage state, with a bias current greater than the junction's critical current, the junction's gauge-invariant phase difference ''overturns,'' and the junction's dynamical behavior is described by a limit cycle in phase space. It is reasonable, then, to ask if there is some connection between arrays of coupled JJ's and the Kuramoto models, which were proposed to study weakly coupled limit-cycle oscillators. In the mid 1990s it was shown that a *serial* array of zero-capacitance, i.e., overdamped, junctions coupled to a load could be mapped onto the GKM [17,18]. The load in this case was essential to provide the coupling between the junctions. This work was based on an averaging process, in which (at least) two distinct time scales of operation were identified: the ''fast'' time scale set by the overturning speed of the individual junctions, and a ''slow'' time scale over which junctions synchronize their overturning rates. By integrating the resistively shunted junction (RSJ) equations describing the dynamics of the junctions over one cycle of the fast motion what remained was the slow dynamics, which described the synchronization behavior of the array.

It was shown in Ref. [17] that a spread in the junction critical currents in the serial array corresponded to a spread in the bare frequencies, Ω_j, of the oscillators in the GKM. Also, the oscillator coupling strength α in the GKM was found to depend on both the dc bias current driving the array and on the impedance of the load. This coupling resulted in each oscillator's time-averaged angular velocity, $\langle d\theta_j/dt\rangle_t$, being renormalized from the bare value it would have had in the absence of coupling. Using well-known methods of analyzing the GKM, the authors of Ref. [17] were able to predict the fraction of the junctions whose renormalized angular velocities had locked to a common value as a function of the dc bias current and the spread in the junction critical currents. (Such locked junctions will be described as *frequency synchronized* throughout this paper.) In part, this mapping between the serial JJ array and the GKM is significant, because it brings to bear upon the problem of understanding the dynamics of the JJ array all that is known about the Kuramoto models, which is substantial. For example, the authors of Ref. [17] were able, based on the GKM, to predict the level of critical current disorder the array could tolerate before frequency synchronization of all N junctions in the array would be lost.

It is an interesting question whether any other JJ array geometries can be mapped onto Kuramoto-like models. Such a connection could indeed prove valuable in shedding light on the synchronization properties of such an array. In fact, the main result of this paper is to show that a *ladder* array of overdamped junctions can be mapped, under appropriate conditions, onto a Kuramoto model with *nearest neighbor*, sinusoidal couplings. Specifically, we consider a ladder of junctions biased horizontally with dc bias currents I_B which are greater than the critical currents of each of the horizontal junctions (see Fig. 1). The junctions are disordered, with individual critical currents $I_{ch,j}$ and resistances $R_{h,j}$ (for the horizontal junctions), and with a spread of critical currents $\Delta=(I_{ch,\max}-\langle I_{ch}\rangle)/\langle I_{ch}\rangle$, where $\langle I_{ch}\rangle$ is the arithmetic mean of the horizontal junction critical currents. Initially, we restrict ourselves to the case of overdamped junctions, with zero internal capacitance, but in the final section of this paper we will present some preliminary results on synchronization in underdamped ladders. We consider both periodic and open boundary conditions, and we study arrays with $N\geqslant 5$. We

find for sufficiently large bias currents, $I_B/\langle I_{ch}\rangle \gtrsim 3$, and critical current disorder up to about 10%, $\Delta \lesssim 0.1$, that the averaged RSJ equations for the ladder reduce to the LKM. As discussed previously, the LKM is not as well studied as the GKM; nevertheless, this result tells us that all our understanding of the dynamical behavior of solutions to the LKM should apply to the ladder array of Josephson junctions. Some aspects of this behavior will be discussed in this paper.

This paper is organized as follows. In Sec. II we discuss the RSJ equations describing the disordered ladder array, talk briefly about measuring the degree of frequency (FS) and phase synchronization (PS) in the array, and discuss a set of assumptions that in turn allow us to perform the averaging process on the RSJ equations. In Sec. III we discuss the averaging procedure for the ladder that results in the LKM. We also compare the levels of FS and PS of the two models, namely, the RSJ model and the LKM, to verify the validity of our averaging process. In Sec. IV we discuss some of the properties of the LKM itself. In Sec. V we look at the effects of thermal noise on the synchronization behavior of the RSJ model and the LKM. In Sec. VI we present some preliminary results on synchronization in the underdamped ladder, in which we assume each junction has an internal capacitance C_j. Our results in Sec. VI are based on the resistively and capacitively shunted junction model (RCSJ model), and we find that for sufficiently large junction capacitance, the frequency synchronization transition, which is a continuous function of the coupling strength α in the overdamped array, is discontinuous in the underdamped ladder. Such behavior has been observed in the PS of the underdamped GKM [19]. Finally, in Sec. VII we conclude and discuss possible avenues for future work.

II. PRELUDE TO AVERAGING

A. RSJ equations

Consider the geometry of Fig. 1, which depicts open boundary conditions, N horizontal junctions, and uniform, horizontal dc bias currents, I_B. The Josephson phase difference across the jth horizontal junction is denoted by ϕ_j, while the phase difference across the left(right) vertical junction in the jth plaquette is $\psi_{l,j}(\psi_{r,j})$. The critical current of the jth horizontal junction is $I_{ch,j}$, while the critical current of the left(right) vertical junction in the jth plaquette is $I_{cl,j}(I_{cr,j})$. The junction's resistance is denoted by $R_{h,j}$, $R_{l,j}$, and $R_{r,j}$ for the horizontal, left, and right junctions, respectively, in the jth plaquette. Conservation of charge applied to the superconducting node (nodes are denoted by filled circles in Fig. 1) on the left and right side, respectively, of the jth horizontal junction yields

$$I_B - I_{ch,j}\sin\phi_j - \frac{\hbar}{2eR_{h,j}}\frac{d\phi_j}{dt} - I_{cl,j}\sin\psi_{l,j} - \frac{\hbar}{2eR_{l,j}}\frac{d\psi_{l,j}}{dt} + I_{cl,j-1}\sin\psi_{l,j-1} + \frac{\hbar}{2eR_{l,j-1}}\frac{d\psi_{l,j-1}}{dt} = 0, \tag{2a}$$

$$-I_B + I_{ch,j}\sin\phi_j + \frac{\hbar}{2eR_{h,j}}\frac{d\phi_j}{dt} - I_{cr,j}\sin\psi_{r,j} - \frac{\hbar}{2eR_{r,j}}\frac{d\psi_{r,j}}{dt} + I_{cr,j-1}\sin\psi_{r,j-1} + \frac{\hbar}{2eR_{r,j-1}}\frac{d\psi_{r,j-1}}{dt} = 0, \tag{2b}$$

where we used the voltage-phase relation for a Josephson junction, $V=(\hbar/2e)d\phi/dt$. Note that Eq. (2) also applies to the four nodes at the ends of the array, i.e., $j=1$ and $j=N$, if we let $\psi_{l,0}(\psi_{r,0})=0$ and $\psi_{l,N}(\psi_{r,N})=0$.

We find it convenient to sort all junctions into one of two groups: horizontal and vertical junctions. We let $\langle I_{ch}\rangle(\langle I_{cv}\rangle)$ denote the arithmetic mean of the horizontal-(vertical) junction critical currents. We also assume that a particular junction's critical current is proportional to the junction area, while its resistance is inversely proportional to its area such that the product of these quantities is the same for all junctions [20]. So we have the following equality for the horizontal junctions:

$$I_{ch,j}R_{h,j} = \langle I_{ch}\rangle\langle R_h\rangle = X_h, \tag{3}$$

for some constant X_h, and where $\langle R_h\rangle$ is the average resistance of the horizontal junctions. One can think of Eq. (3) as defining the ratio $R_{h,j}/\langle R_h\rangle = (I_{ch,j}/\langle I_{ch}\rangle)^{-1}$, where the value of $I_{ch,j}/\langle I_{ch}\rangle$ is generated by a suitable random number generator. Likewise for the vertical junctions we have

$$I_{cl,j}R_{l,j} = I_{cr,j}R_{r,j} = \langle I_{cv}\rangle\langle R_v\rangle = X_v. \tag{4}$$

In the dimensionless version of Eq. (2) [see Eq. (6) below], the ratio X_h/X_v appears. This can be set as desired, including to a value of unity.

To write Eq. (2) in dimensionless form, we divide by $\langle I_{ch}\rangle$, define a dimensionless time

$$\tau \equiv \frac{t}{(\hbar/2e\langle I_{ch}\rangle\langle R_h\rangle)},$$

and a dimensionless bias current $i_B \equiv I_B/\langle I_{ch}\rangle$. Note that we divide by the average critical current for the *horizontal* junctions, since these are the most important junctions for our horizontal biasing scheme. We also define dimensionless critical currents as follows: $i_{ch,j} \equiv I_{ch,j}/\langle I_{ch}\rangle$, $i_{cl,j} \equiv I_{cl,j}/\langle I_{cv}\rangle$, and $i_{cr,j} \equiv I_{cr,j}/\langle I_{cv}\rangle$. Of particular importance in our analysis is a dimensionless "coupling" constant

$$\alpha \equiv \frac{\langle I_{cv}\rangle}{\langle I_{ch}\rangle} = \frac{\langle R_h\rangle}{\langle R_v\rangle}\frac{X_v}{X_h}, \tag{5}$$

where we used Eqs. (3) and (4) to obtain the second term on the right side. Then Eq. (2) becomes

$$i_B - i_{ch,j}\sin\phi_j - i_{ch,j}\frac{d\phi_j}{d\tau} - \alpha i_{cl,j}\sin\psi_{l,j} - \alpha\left(\frac{X_h}{X_v}\right)i_{cl,j}\frac{d\psi_{l,j}}{d\tau} + \alpha i_{cl,j-1}\sin\psi_{l,j-1} + \alpha\left(\frac{X_h}{X_v}\right)i_{cl,j-1}\frac{d\psi_{l,j-1}}{d\tau} = 0, \tag{6a}$$

$$-i_B+i_{ch,j}\sin\phi_j+i_{ch,j}\frac{d\phi_j}{dt}-\alpha i_{cr,j}\sin\psi_{r,j}$$
$$-\alpha\left(\frac{X_h}{X_v}\right)i_{cr,j}\frac{d\psi_{r,j}}{dt}+\alpha i_{cr,j-1}\sin\psi_{r,j-1}$$
$$+\alpha\left(\frac{X_h}{X_v}\right)i_{cr,j-1}\frac{d\psi_{r,j-1}}{dt}=0. \tag{6b}$$

Equation (6) is supplemented with the constraint of fluxoid quantization in the absence of any external magnetic flux or induced flux due to currents in the plaquettes. For the jth plaquette this additional constraint yields

$$\phi_j+\psi_{r,j}-\phi_{j+1}-\psi_{l,j}=0, \quad 1\leqslant j\leqslant N-1. \tag{7}$$

Equations (6) and (7) allow us to solve numerically for the $3N-2$ phases: ϕ_j, $\psi_{r,j}$, and $\psi_{l,j}$ [21].

As mentioned in Sec. I, we have also considered periodic boundary conditions. In that case, we imagine the ends of the ladder shown in Fig. 1 connected together, resulting in an array with $N-1$ ''horizontal'' junctions and $N-1$ plaquettes. In Eqs. (6) and (7) the index j then satisfies $1\leqslant j\leqslant N-1$ and $\psi_{l,0}(\psi_{r,0})=\psi_{l,N-1}(\psi_{r,N-1})$, while $\phi_N=\phi_1$.

Also of importance is how the critical currents are assigned. We consider two cases, a random and a nonrandom method. In assigning the critical currents randomly, we generate values according to a parabolic probability distribution function (pdf) of the form

$$P(i_c)=\frac{3}{4\Delta^3}[\Delta^2-(i_c-1)^2], \tag{8}$$

where i_c generically represents a dimensionless critical current for either the horizontal or vertical junctions that is normalized by the appropriate average $i_c=I_c/\langle I_c\rangle$ and Δ determines the spread of the critical currents. Equation 8 results in critical currents in the range $1-\Delta\leqslant i_c\leqslant 1+\Delta$. Also note that this choice (also used in Ref. [17]) for the pdf avoids problems associated with more extreme critical currents that are occasionally generated with pdfs with tails. We generally allow for up to 10% disorder, i.e., $0\leqslant\Delta\leqslant 0.1$. In addition, a *nonrandom* method for assigning critical currents was applied only to the horizontal junctions and was based on the expression

$$i_{ch,j}=1+\Delta-\frac{2\Delta}{(N-1)^2}[4j^2-4(N+1)j+(N+1)^2], \tag{9}$$

which results in the values of $i_{ch,j}$ varying quadratically as a function of position along the ladder, while $1-\Delta\leqslant i_{ch,j}\leqslant 1+\Delta$.

B. Results for the RSJ equations

It is helpful to show some typical synchronization behavior in this system. Using a fourth-order Runge-Kutta algorithm, we solved Eqs. (6) and (7) numerically for the phase differences ϕ_j, $\psi_{l,j}$, and $\psi_{r,j}$ and the dimensionless voltages (or, in the language of rotators, angular velocities) $d\phi_j/d\tau$, $d\psi_{l,j}/d\tau$, and $d\psi_{r,j}/d\tau$. We used a time step of $\Delta\tau=0.01$, and we initialized the phases randomly between 0 and 2π. We measured the degree of FS of the *horizontal* junctions (rotators) simply by calculating the standard deviation of their time-averaged voltages (angular velocities). For simplicity, let $\omega_j\equiv\langle d\phi_j/d\tau\rangle_\tau$ (where angular brackets with the subscript τ denote time averaging). Then the standard deviation is simply

$$\sigma_\omega=\sqrt{\frac{\sum_{j=1}^{N}(\omega_j-\langle\omega\rangle)^2}{N-1}}, \tag{10}$$

where $\langle\omega\rangle$ is the arithmetic mean of the time-averaged angular velocities of the horizontal junctions, i.e. $\langle\omega\rangle=(\Sigma_j\omega_j)/N$. To calculate ω_j numerically we ran our code for 2.5×10^5 time steps (of the order of 1000 rotator periods) before averaging over an additional 2.5×10^5 time steps. In some sense, one can think of σ_ω as a type of inverse frequency synchronization order parameter, since full frequency synchronization of the horizontal junctions is signaled by a very small value of σ_ω, typically less than 10^{-4} in our numerical results, while a ''large'' value of σ_ω (of order one) means that on average the horizontal junctions' angular velocities are not synchronized.

Typical behavior of σ_ω as a function of α is shown in Fig. 2 for $N=8$ with periodic boundary conditions. The horizontal junctions had randomly assigned critical currents with a spread $\Delta=0.05$. Also, in Fig. 3 we show the time-averaged angular velocities for *each* of the eight horizontal junctions in the periodic ladder. The array exhibits clustering, which is well known to occur in systems of locally coupled oscillators [8–10]. That is, the averaged angular velocities of the individual rotators adjust themselves as the value of the ''coupling constant'' α increases, and groups or clusters of rotators form which have identical averaged angular velocities. This continues until eventually only two clusters exist in the array, and at a critical value α_c, the two clusters merge and full FS occurs. For $\alpha\geqslant\alpha_c$ we find that $\sigma_\omega\lesssim10^{-4}$. Note that the behavior depicted in Fig. 3 is a smooth function of α, which we remind the reader is the ratio of the average critical currents of the vertical to the horizontal junctions.

We measure the PS of the horizontal junctions by the famous Kuramoto order parameter [2]

$$r\equiv\frac{1}{N}\sum_{j=1}^{N}e^{i\phi_j}. \tag{11}$$

Since r is complex and time dependent, we calculate $\langle|r|\rangle_\tau$, the time average of the modulus of r. We are interested in the behavior of $\langle|r|\rangle_\tau$ as a function of α. Full PS of the junctions is denoted by $\langle|r|\rangle_\tau\to1$, while $\langle|r|\rangle_\tau\approx0$ means the ϕ_j are basically distributed randomly between 0 and 2π. Figure 2(b) demonstrates a typical behavior of the $\langle|r|\rangle_\tau$. Note that for $\alpha<\alpha_c$, $\langle|r|\rangle_\tau$ varies in a complicated manner, and only

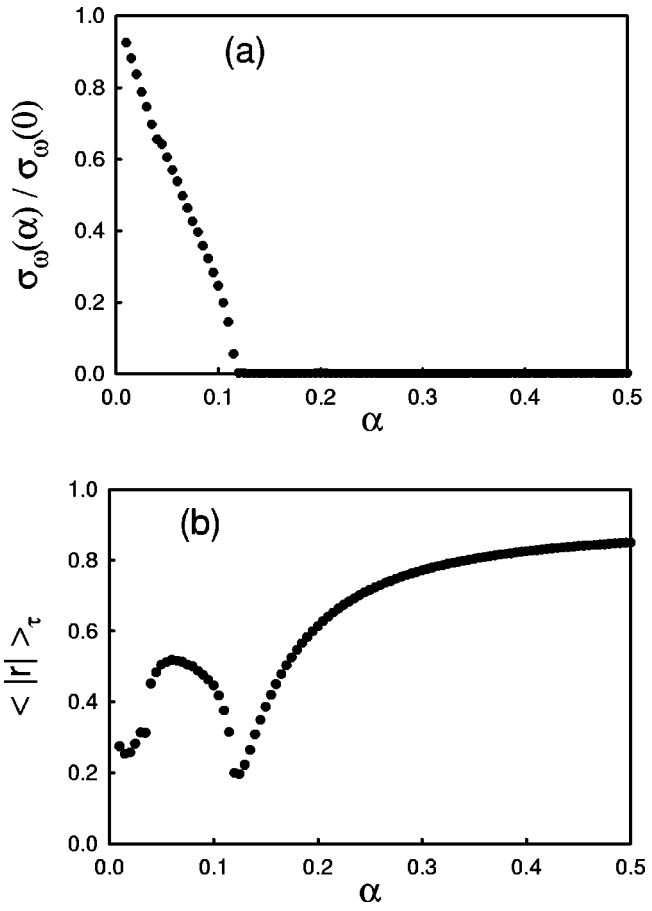

FIG. 2. Frequency and phase synchronization in an 8-plaquette overdamped ladder with periodic boundary conditions [see Eq. (6)]. The bias current was $i_B = I_B / \langle I_{ch} \rangle = 5$, and the critical currents of the horizontal junctions were assigned randomly according to Eq. (8) with a spread of $\Delta = 0.05$. The vertical junctions were not disordered, and the value of the ratio X_h / X_v in Eq. (6) was set to one. (a) Standard deviation of average angular velocities (or voltages in our dimensionless units) of the horizontal junctions, σ_ω, scaled by its value at zero coupling. (b) Time-averaged modulus of the Kuramoto order parameter, which measures the degree of phase synchronization of the junctions. $\langle |r| \rangle_\tau$ is a complicated function of α for $\alpha < \alpha_c$ and then grows smoothly as α is increased beyond α_c, asymptotically approaching one for very large α. Qualitatively similar behavior is observed for arrays with open boundary conditions.

for $\alpha > \alpha_c$ does $\langle |r| \rangle_\tau$ grow smoothly with α, with $\langle |r| \rangle_\tau$ asymptotically approaching unity for sufficiently large α. It is clear from Fig. 2 that full FS is much easier to obtain than full PS in the sense that a smaller value of α is required for FS than PS. We find it useful to envision the motion of the phases of these rotators as points moving around the unit circle. Frequency synchronized motion means that the phase points all move with same average angular velocity, but if those points are distributed broadly around the unit circle, the degree of PS will be low. To obtain high degrees of both frequency *and* phase synchronization requires both that the phase points move with the same average angular velocity and that they remain clustered at roughly the same location

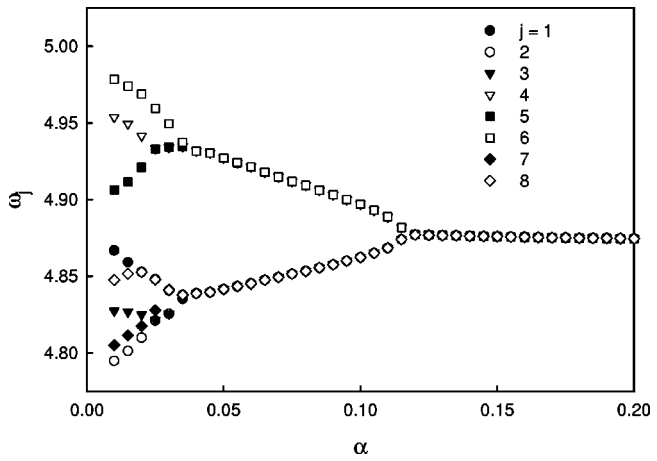

FIG. 3. Clustering of the time-averaged angular velocities for the periodic ladder depicted in Fig. 2. The critical currents of the rung junctions $i_{ch,j}$ result in bare angular frequencies Ω_j according to Eq. (18). The value of α_c is easily seen to be slightly greater than 0.1.

on the unit circle as they move. We observe qualitatively the same behavior for ladders with open boundary conditions.

C. Some simplifying assumptions

To obtain the averaged version of Eqs. (6) and (7) we find it useful to make three assumptions, which we describe in turn. In each case, we discuss the validity or appropriateness of each assumption.

Assumption 1. Only the horizontal junctions are disordered. That is, all vertical junctions have identical critical currents and resistances,

$$I_{cl,j} = I_{cr,j} \equiv I_{cv},$$

$$R_{l,j} = R_{r,j} \equiv R_v,$$

where $I_{cv} R_v = X_v$. For simplicity, we assume $X_h / X_v = 1$ so that

$$I_{ch,j} R_{h,j} = I_{cv} R_v \quad 1 \leq j \leq N.$$

This assumption makes the averaging process tractable. Perhaps more importantly, we have made some checks of the effects of this assumption as follows: we calculated σ_ω for the averaged equations [see Eq. (26) below], for the RSJ equations with *no* vertical junction disorder (as based on assumption 1), and also for the fully disordered RSJ equations, where both horizontal and vertical junctions are disordered. For the sake of space, those results are not shown here, but we found no qualitative difference among all three sets of results for $N = 15$, $i_B = 5$, and $\Delta = 0.1$. It would appear that, at least for moderate or small amounts of disorder, i.e., $\Delta \lesssim 0.1$, the synchronization behavior of the array is not strongly affected by this assumption.

Assumption 2. A special phase relationship between vertical junctions. We assume the phase differences across the two vertical junctions in the jth plaquette are related by

$$\psi_{r,j} = -\psi_{l,j} + 2\pi n, \tag{12}$$

for any integer n. This relationship is known to be true in the ladder in the absence of disorder [22], but it is not *a priori* obvious that it holds in the disordered ladder. To test the validity of Eq. 12 we have calculated $(\psi_{r,j}+\psi_{l,j})/2\pi$ as a function of time based on Eqs. (6) and (7) (along with assumption 1) for $N=5$, looking at both periodic and open boundary conditions, and for various sets of critical currents and initial phase differences. If Eq. (12) is satisfied, such a plot should give the value of the integer n. We do find complicated behavior in the sense that the details of the temporal behavior of $(\psi_{r,j}+\psi_{l,j})/2\pi$ are dependent upon the particular configuration of critical currents, initial phase differences, as well as the value of α, but a general trend is observable. For large bias currents, $i_B \gtrsim 3$, we find Eq. (12) is satisfied except for phase slips of very short duration. These slips occur only for $\alpha < \alpha_c$, i.e., prior to the onset of full FS, and are transient in that they disappear after a sufficiently long time τ^*, where we find $\tau^* \lesssim 2500$. For lower bias currents, however, such as $i_B = 1.5$, and for $\alpha < \alpha_c$, the phase slips do not appear to be transient, or are at least transient with a very long decay time. For $\alpha > \alpha_c$ and $i_B = 1.5$, no such slips occur, as was also seen at higher bias currents. Thus, after careful study of the temporal behavior of $(\psi_{r,j}+\psi_{l,j})/2\pi$, we are led to the conclusion that Eq. (12) is a reasonable approximation for sufficiently large bias currents, $i_B \gtrsim 3$, as long as a sufficient time interval $\tau' > \tau^*$ is allowed for transients to die out before any temporal averages are calculated. We find a value of $\tau' = 2500$ to be reasonable.

Note that in the light of assumption 2 we can simplify Eq. (7) to

$$\psi_{l,j} = \frac{\phi_j - \phi_{j+1} + 2\pi n}{2}.$$

Substituting this expression into Eq. (6a), and taking assumption 1 into account, leads to the expression

$$i_{ch,j}\frac{d\phi_j}{d\tau} + \frac{\alpha}{2}\left[\frac{d\phi_{j+1}}{d\tau} - 2\frac{d\phi_j}{d\tau} + \frac{d\phi_{j-1}}{d\tau}\right] = i_B - i_{ch,j}\sin\phi_j + \alpha\sin\left(\frac{\phi_{j+1}-\phi_j}{2}\right) + \alpha\sin\left(\frac{\phi_{j-1}-\phi_j}{2}\right), \tag{13}$$

where we have taken $X_v/X_h = 1$ for simplicity. Note that Eq. (6b) can also be simplified in light of assumption 1. The result is an equation in terms of the phases ϕ_j and $\psi_{r,j}$. Since we are primarily interested in the behavior of the horizontal junctions, Eq. (13) is the natural one to use.

Assumption 3. Ignore the discrete Laplacian. In Eq. (13) we drop the terms $d\phi_{j+1}/d\tau - 2d\phi_j/d\tau + d\phi_{j-1}/d\tau \equiv \nabla^2(d\phi_j/d\tau)$. We find, over a wide range of bias currents, that $\nabla^2(d\phi_j/d\tau)$ oscillates with an amplitude that depends on the value of i_B and α, but always with a time-averaged value of approximately zero. Note that, meanwhile, the first term on the left side of Eq. (13) has a nonzero time average. Since $\langle \nabla^2(d\phi_j/d\tau)\rangle_\tau \approx 0$ and we are interested in the time-averaged behavior of Eq. (13) it seems reasonable to drop the term.

As a result of all three assumptions we are left with the following equation describing the dynamics of the phase differences across the horizontal junctions:

$$\frac{d\phi_j}{d\tau} = \frac{i_B}{i_{ch,j}} - \sin\phi_j + \frac{\alpha}{i_{ch,j}}\sum_{\delta=\pm 1}\sin\left(\frac{\phi_{j+\delta}-\phi_j}{2}\right). \tag{14}$$

It is now straightforward to see that $\alpha/i_{ch,j}$ plays the role of the coupling strength between neighboring junctions. The next step is to average Eq. (14).

III. AVERAGING THE RSJ EQUATIONS

The work in this section is based on a technique used previously to average the RSJ equations for a current-biased *serial* array of overdamped JJ's connected to a load [23], but we emphasize that no load is required for the horizontal junctions of the ladder array to synchronize. The first step is to transform the phase variables ϕ_j, which move around the unit circle with a nonzero angular acceleration, to a new variable θ_j, which increases with time with a constant angular velocity Ω_j, in the uncoupled limit [3]. This transformation follows from Eq. (14) in the $\alpha = 0$ limit,

$$\theta_j = \int \frac{d\phi_j}{\left(\frac{d\phi_j}{d\tau}\right)_{\alpha=0}} = \int \frac{d\phi_j}{\frac{i_B}{i_{ch,j}} - \sin\phi_j} = \int \frac{d\phi_j}{\mathcal{I}_j - \sin\phi_j}, \tag{15}$$

where we defined the quantity $\mathcal{I}_j \equiv i_B/i_{ch,j}$ for convenience. The integral gives an expression for the new phase variable θ_j in terms of the original phases ϕ_j,

$$\theta_j = \frac{2}{\sqrt{\mathcal{I}_j^2 - 1}}\tan^{-1}\left[\sqrt{\frac{\mathcal{I}_j+1}{\mathcal{I}_j-1}}\tan\left(\frac{\phi_j}{2}+\frac{\pi}{4}\right)\right], \tag{16}$$

which can be inverted to give ϕ_j in terms of θ_j,

$$\phi_j = 2\tan^{-1}\left[\sqrt{\frac{\mathcal{I}_j+1}{\mathcal{I}_j-1}}\tan\left(\frac{\theta_j}{2}\right)\right] - \frac{\pi}{2}. \tag{17}$$

At this point it is also useful to calculate the angular velocity of each junction or rotator in the absence of coupling, Ω_j. If T_j is the period of the jth rotator when uncoupled, then

$$T_j = \frac{2\pi}{\Omega_j} = \int_0^{T_j} d\tau = \int_0^{2\pi} \frac{d\phi_j}{\left(\frac{d\phi_j}{d\tau}\right)_{\alpha=0}} = \int_0^{2\pi} \frac{d\phi_j}{\mathcal{I}_j - \sin\phi_j},$$

which gives

$$\Omega_j = \sqrt{\mathcal{I}_j^2 - 1} = \sqrt{\left(\frac{i_B}{i_{ch,j}}\right)^2 - 1}. \tag{18}$$

Note that for large bias currents, $\Omega_j \approx i_B/i_{ch,j}$.

The next step is to express Eq. (14) in terms of the new phase variables θ_j. We write

$$\frac{d\theta_j}{d\tau}=\frac{d\theta_j}{d\phi_j}\cdot\frac{d\phi_j}{d\tau},$$

where $d\theta_j/d\phi_j$ follows from Eq. (16) and $d\phi_j/d\tau$ from Eq. (14). One must also remember that ϕ_j is expressed in terms of θ_j via Eq. (17). We find

$$\frac{d\theta_j}{d\phi_j}=\frac{\sqrt{\mathcal{I}_j^2-1}}{\mathcal{I}_j-\sin\phi(\theta_j)}=\frac{\Omega_j}{\mathcal{I}_j-\sin\phi(\theta_j)},$$

$$\frac{d\theta_j}{d\tau}=\Omega_j\left[1+\left(\frac{\alpha}{i_{ch,j}}\right)\frac{1}{\mathcal{I}_j-\sin\phi(\theta_j)}\times\sum_{\delta=\pm1}\sin\left(\frac{\phi(\theta_{j+\delta})-\phi(\theta_j)}{2}\right)\right]. \tag{19}$$

A shift of the phases is also convenient,

$$\tilde{\theta}_j\equiv\theta_j-\Omega_j\tau. \tag{20}$$

Thus $\tilde{\theta}_j$ measures by how much the phase variable θ_j differs from the value it would have in the absence of coupling. Equation (19) then becomes

$$\frac{d\tilde{\theta}_j}{d\tau}=\left(\frac{\alpha}{i_{ch,j}}\right)\frac{\Omega_j}{\mathcal{I}_j-\sin\phi(\tilde{\theta}_j+\Omega_j\tau)}\times\sum_{\delta=\pm1}\sin\left[\frac{\phi(\tilde{\theta}_{j+\delta}+\Omega_{j+\delta}\tau)-\phi(\tilde{\theta}_j+\Omega_j\tau)}{2}\right]. \tag{21}$$

The bare angular velocities Ω_j have a percent variation across the array of the order of Δ (see Fig. 3). For moderate to small amounts of disorder it is reasonable to make the following replacements in the arguments of the sine functions in Eq. (21):

$$\phi(\tilde{\theta}_j+\Omega_j\tau)\to\phi(\tilde{\theta}_j+\langle\Omega\rangle\tau),$$

where $\langle\Omega\rangle=(\Sigma_j\Omega_j)/N$. Then it is also convenient to rescale the time variable $\tau'\equiv\langle\Omega\rangle\tau$. Equation (21) becomes

$$\frac{d\tilde{\theta}_j}{d\tau'}=\left(\frac{\alpha}{i_{ch,j}}\right)\frac{\Omega_j}{\langle\Omega\rangle}\frac{1}{\mathcal{I}_j-\sin\phi(\tilde{\theta}_j+\tau')}\times\sum_{\delta=\pm1}\sin\left[\frac{\phi(\tilde{\theta}_{j+\delta}+\tau')-\phi(\tilde{\theta}_j+\tau')}{2}\right]. \tag{22}$$

The next key idea is to treat $\tilde{\theta}_j$, the "slow" variable, as constant for the duration of one cycle of the "fast" variable τ'. We then average Eq. (22) over one cycle of τ'.

$$\left\langle\frac{d\tilde{\theta}_j}{d\tau'}\right\rangle_{\text{fast}}=\left(\frac{\alpha}{i_{ch,j}}\right)\frac{\Omega_j}{\langle\Omega\rangle}\sum_{\delta=\pm1}\frac{1}{2\pi}\int_0^{2\pi}\frac{1}{\mathcal{I}_j-\sin\phi(\tilde{\theta}_j+\tau')}\times\sin\left[\frac{\phi(\tilde{\theta}_{j+\delta}+\tau')-\phi(\tilde{\theta}_j+\tau')}{2}\right]d\tau',$$

where the angular brackets on the left side denote the result of the averaging process. Next, let $\Psi_\delta\equiv\tilde{\theta}_{j+\delta}-\tilde{\theta}_j$. Also, since the $\tilde{\theta}_j$ are treated as constants during the integration, they can be absorbed into the definition of τ', i.e., $\tau'\to\tau'+\tilde{\theta}_j$ to give

$$\left\langle\frac{d\tilde{\theta}_j}{d\tau'}\right\rangle_{\text{fast}}=\left(\frac{\alpha}{i_{ch,j}}\right)\frac{\Omega_j}{\langle\Omega\rangle}\sum_{\delta=\pm1}\frac{1}{2\pi}\int_0^{2\pi}\frac{1}{\mathcal{I}_j-\sin\phi(\tau')}\times\sin\left[\frac{\phi(\Psi_\delta+\tau')-\phi(\tau')}{2}\right]d\tau'. \tag{23}$$

Making use of Eqs. (15) through (17), and after some algebra we obtain the two useful relations

$$\mathcal{I}_j-\sin\phi(\tau')=\frac{\Omega_j^2}{\mathcal{I}_j-\cos\tau'},$$

$$\sin\left[\frac{\phi(\Psi_\delta+\tau')-\phi(\tau')}{2}\right]=\frac{\Omega_j\sin\left(\frac{\Psi_\delta}{2}\right)}{\sqrt{(\mathcal{I}_j-\cos\tau')(\mathcal{I}_j-\cos[\Psi_\delta+\tau'])}}.$$

In light of these results, Eq. (23) can be written as

$$\left\langle\frac{d\tilde{\theta}_j}{d\tau'}\right\rangle_{\text{fast}}=\left(\frac{\alpha}{i_{ch,j}}\right)\frac{\sin\left(\frac{\Psi_\delta}{2}\right)}{\langle\Omega\rangle}\sum_{\delta=\pm1}\frac{1}{2\pi}\times\int_0^{2\pi}\sqrt{\frac{\mathcal{I}_j-\cos\tau'}{\mathcal{I}_j-\cos(\Psi_\delta+\tau')}}\,d\tau'. \tag{24}$$

Since we are interested in the limit of large bias currents, we expand the integrand in powers of $1/\mathcal{I}_j$. (Recall that $\mathcal{I}_j\equiv i_B/i_{ch,j}$.)

$$\sqrt{\frac{\mathcal{I}_j-\cos\tau'}{\mathcal{I}_j-\cos(\Psi_\delta+\tau')}}=1+\frac{1}{2\mathcal{I}_j}[\cos(\Psi_\delta+\tau')-\cos\tau']+\frac{1}{8\mathcal{I}_j^2}[3\cos^2(\Psi_\delta+\tau')-2\cos\tau'\cos(\Psi_\delta+\tau')-\cos^2\tau']+\mathcal{O}\left(\frac{1}{\mathcal{I}_j^3}\right).$$

Substituting into Eq. (24) and integrating order by order gives, to order $1/\mathcal{I}_j^2$,

$$\left\langle \frac{d\tilde{\theta}_j}{d\tau'} \right\rangle_{\text{fast}} = \frac{1}{\langle\Omega\rangle}\left(\frac{\alpha}{i_{ch,j}}\right)\sum_{\delta=\pm1}\left[\sin\left(\frac{\Psi_\delta}{2}\right)+\frac{1}{4\mathcal{I}_j^2}\sin^3\left(\frac{\Psi_\delta}{2}\right)\right],$$

where the term of $\mathcal{O}(1/\mathcal{I}_j)$ vanished upon integration over τ'. Transferring back to the original time variable τ and to the phase variable $\theta_j=\tilde{\theta}_j+\Omega_j\tau$, and making use of the approximation $\Psi_\delta=\tilde{\theta}_{j+\delta}-\tilde{\theta}_j\approx\theta_{j+\delta}-\theta_j$, where the last approximation should be valid for moderate to small amounts of disorder, we finally arrive at the averaged version of the RSJ equations, expressed to $\mathcal{O}(1/\mathcal{I}_j^2)$,

$$\left\langle \frac{d\theta_j}{d\tau'} \right\rangle_{\text{fast}} = \Omega_j+\left(\frac{\alpha}{i_{ch,j}}\right)\sum_{\delta=\pm1}\left[\sin\left(\frac{\theta_{j+\delta}-\theta_j}{2}\right)+\frac{1}{4\mathcal{I}_j^2}\sin^3\left(\frac{\theta_{j+\delta}-\theta_j}{2}\right)\right]. \quad (25)$$

Equation (25) is the main result of this paper. However, for large bias currents, $\mathcal{I}_j^2\gg1$, we can drop the term of $\mathcal{O}(1/\mathcal{I}_j^2)$ and reduce Eq. (25) to an expression that is of $\mathcal{O}(1)$ in terms of the $\mathcal{I}_j$:

$$\left\langle \frac{d\theta_j}{d\tau'} \right\rangle_{\text{fast}} = \Omega_j+\left(\frac{\alpha}{i_{ch,j}}\right)\sum_{\delta=\pm1}\sin\left(\frac{\theta_{j+\delta}-\theta_j}{2}\right). \quad (26)$$

Note that with a simple rescaling: $\theta_j\to2\theta_j$, $\Omega_j\to2\Omega_j$, and $\alpha\to2\alpha$, Eq. (26) has the standard form of the LKM [9], namely,

$$\frac{d\theta_j}{d\tau}=\Omega_j+K_j\sum_{\delta=\pm1}\sin(\theta_{j+\delta}-\theta_j),$$

where $K_j\equiv\alpha/i_{ch,j}$.

As a test of the validity of Eq. (26) for describing the synchronization behavior of the JJ ladder, we compare the values of the quantities σ_ω and $\langle|r|\rangle_\tau$ calculated numerically from Eq. (26) as well as Eqs. (6) and (7). Figure 4 shows such a comparison for $N=15$ horizontal junctions and a bias current of $i_B=5$ for periodic boundary conditions. The critical currents were assigned *nonrandomly* with a spread of $\Delta=0.05$. Each plot in Fig. 4 was obtained by averaging over five sets of initial phases, and the error bars were smaller than the sizes of the symbols. (We see qualitatively similar behavior for the case of open boundary conditions.) In Fig. 4(a) a well-defined critical coupling α_c for full FS can be identified, and the LKM and the RSJ results for α_c are in very good agreement just by visual inspection of the graphs. Likewise, the degree of PS between the two models are in excellent agreement. In particular the LKM, like the RSJ model, points to the much larger coupling strengths needed for both full FS and PS compared to the coupling needed for FS alone. To be more specific, if we define full PS by the condition $\langle|r|\rangle_\tau\geqslant0.99$, and then also define α_c' to be the minimum value of the coupling for this condition to be satisfied, then both the LKM and the RSJ models tell us that α_c' is considerably larger than α_c. We have also studied the agreement between the LKM and the RSJ models for the case of *randomly* assigned critical currents and both open and periodic boundary conditions. We find results qualitatively similar to those in Fig. 4.

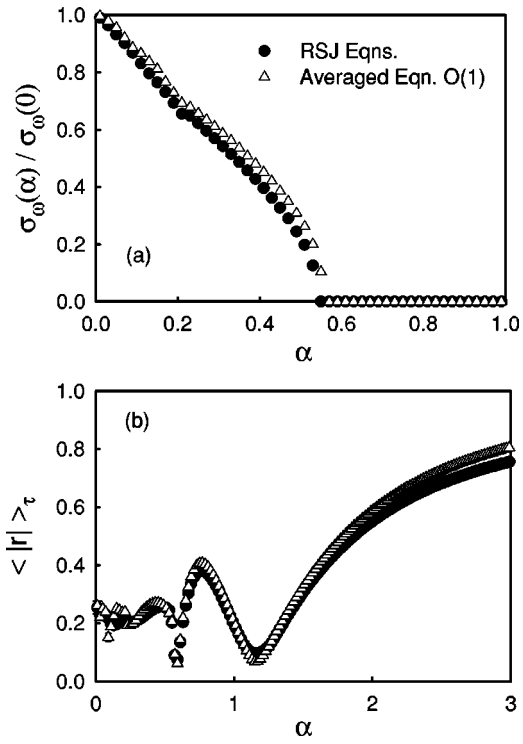

FIG. 4. A comparison of frequency and phase synchronization in the LKM and the RSJ models for the overdamped ladder and periodic boundary conditions. Array consists of $N=15$ horizontal junctions, or rotators, with $i_B=5$, and *nonrandomly* assigned critical currents with $\Delta=0.05$. (a) The scaled standard deviation $\sigma_\omega(\alpha)/\sigma_\omega(0)$. (b) The time-averaged Kuramoto order parameter $\langle|r|\rangle_\tau$. Note the different scales on the horizontal axes of the two graphs.

We have considered other array sizes with $N\neq15$. In general, we find that for $N\geqslant5$, $i_B\gtrsim3$, and both types of boundary conditions, the LKM and RSJ models exhibit a level of agreement similar to that depicted in Fig. 4 for $N=15$.

As discussed in Sec. II we expect the two models to differ more substantially for small bias currents. This behavior is demonstrated in Fig. 5, which compares σ_ω for the LKM and RSJ models for $N=15$ and $i_B=1.5$. Also included are the results for the LKM when the term of order of $1/i_B^2$ is included from Eq. (25). We note that at smaller bias currents, the inclusion of the $1/i_B^2$ term improves the agreement with the RSJ model, but the existence of phase slips in the vertical junctions that violate Eq. (12) is likely the cause of the difference between the averaged and the RSJ equations observed in the figure. In looking at a range of array sizes and at both periodic and open boundary conditions, we find that typically the values of α_c between the averaged and RSJ equations are in agreement within a few percents for $i_B\gtrsim3$.

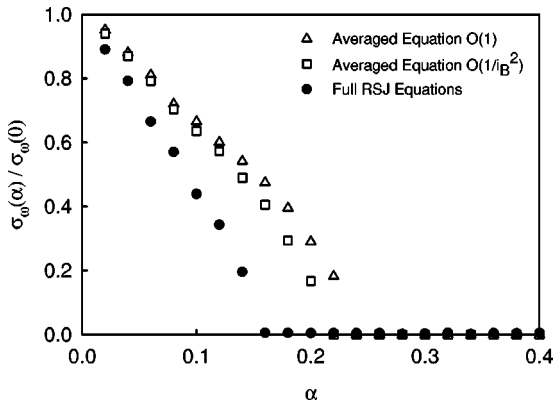

FIG. 5. A comparison of the frequency synchronization in the LKM and the RSJ models for the overdamped ladder with $N=15$ and open boundary conditions, *nonrandom* critical currents with $\Delta=0.05$, and a bias current of $i_B=1.5$. The results based on the $\mathcal{O}(1)$ LKM are shown, as well as the LKM with the inclusion of the term of $\mathcal{O}(1/i_B^2)$. Including the correction term in the averaged equations helps the agreement with the RSJ model. The disagreement with the RSJ model is expected and is likely due to phase slips in the vertical junctions of a plaquette, which is not accounted for in the LKM.

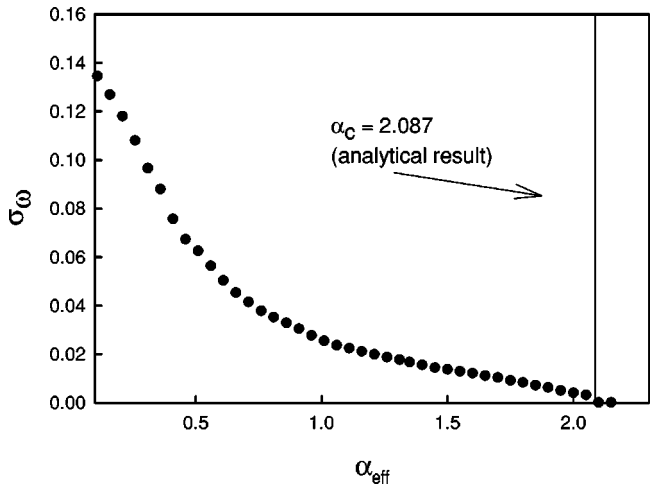

FIG. 6. Frequency synchronization of the LKM, Eq. (26), with $\alpha_{\rm eff}\equiv\alpha/\langle i_{ch}\rangle$, with open boundary conditions, $N=50$, and a comparison with the value of α_c as calculated from Eq. (30). Bare frequencies were assigned randomly according to a parabolic pdf of the structure of Eq. (8) with mean $\langle\Omega\rangle=5$ and spread $\Delta\Omega=0.5$. Note the agreement between the analytic results for α_c and what one would identify from the graph of σ_ω.

IV. BEHAVIOR OF THE LKM

One of the main points of this paper is that, if the slow dynamics of the overdamped ladder are well described by the LKM, then all that is already known about the dynamics of the LKM ought to be applicable to the ladder. In this section we discuss some properties of solutions to the LKM.

Phase slips and voltage bursts near synchronization. It has been demonstrated for the LKM [9] that as the coupling strength α approaches α_c from below, voltage bursts (or angular velocity bursts) and corresponding phase slips occur in the rotators with a time interval between slips that grows as $\alpha\rightarrow\alpha_c^-$ according to $\tau_{\rm slip}\propto 1/\sqrt{\alpha_c-\alpha}$. We have observed this phenomenon of phase slips for the LKM [Eq. (26)]; in particular, we have observed that as $\alpha\rightarrow\alpha_c^-$, the time between the phase slips grows, demonstrating critical slowing down. Such slipping is thus also expected in the RSJ model.

Analytic determination of α_c. It is possible to derive an expression for α_c based on a fixed point analysis of the system of equations formed by taking the difference of Eq. (26) for neighboring rotators. We present here our results for the case of open boundary conditions. The key idea [24] is to consider the quantity $\eta_j\equiv(\theta_{j+1}-\theta_j)/2$. We find that Eq. (26) leads to the set of equations

$$\frac{d\eta_j}{d\tau}=D_j+\frac{\alpha}{\langle i_{ch}\rangle}[\sin(\eta_{j+1})-2\sin(\eta_j)+\sin(\eta_{j-1})],$$

$$1\leqslant j\leqslant N-1, \tag{27}$$

where $\eta_0=0$, $\eta_N=0$, and $D_j\equiv(\Omega_{j+1}-\Omega_j)/2$. Also, we have replaced $i_{ch,j}$ with $\langle i_{ch}\rangle$, the arithmetic mean of the critical currents, in the denominator of the coupling term, an approximation which should be reasonable for moderate to small levels of disorder. Remembering that Eq. (26) already has the "fast" temporal dependence integrated out, we define synchronization of oscillators j and $j+1$ as when $d\eta_j/d\tau=0$. Thus we need to solve for the fixed points of Eq. (27):

$$0=D_j+\frac{\alpha}{\langle i_{ch}\rangle}[u_{j+1}-2u_j+u_{j-1}]\quad 1\leqslant j\leqslant N-1, \tag{28}$$

where $u_j\equiv\sin(\eta_j)$. We find the solution to Eq. (28) that can be written as

$$u_j=\frac{2\langle i_{ch}\rangle}{\alpha(N+1)}\sum_{k=j}^{N}\left[jD_k+\left\{\sum_{n=1}^{j-1}nD_n\right\}\delta_{k,j}\right](N-k+1). \tag{29}$$

A fully frequency synchronized state is denoted by the existence of solutions u_j which fall within the physical range $-1\leqslant u_j\leqslant 1$ for $1\leqslant j\leqslant N-1$. In fact, the value of the critical coupling α_c is the maximum value of α for which one of the u_j, say u_k, is just outside of this range while the u_j ($j\neq k$) are still within this range. So to find α_c we set the magnitude of each of the u_j equal to unity in Eq. (29) and find a corresponding value for $\alpha_{c,j}$. The physical value of the critical coupling is the maximum of the set $\{\alpha_{c,j}\}$, i.e.,

$$\alpha_c=\frac{2\langle i_{ch}\rangle}{N+1}\left|\sum_{k=j}^{N}\left[jD_k+\left\{\sum_{n=1}^{j-1}nD_n\right\}\delta_{k,j}\right](N-k+1)\right|_{\rm max}. \tag{30}$$

For a given set of critical currents and a value of the bias current we determine the set $\{D_j\}$ and then α_c from Eq. (30). Indeed this gives a much more rapid way of finding the critical coupling than solving either the LKM or RSJ model numerically! As a test of the validity of this result, Fig. 6 compares the value of α_c calculated from Eq. (30) with the behavior of σ_ω from a numerical solution of the LKM [Eq.

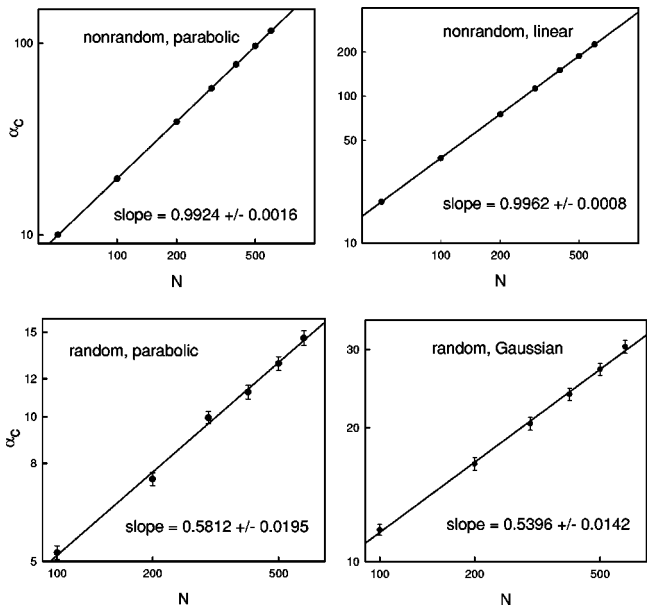

FIG. 7. Log-log plot of α_c [as determined from Eq. (30)] for the LKM as a function of array size N for open boundary conditions and four different methods for assigning the bare frequencies: nonrandomly, according to either a parabolic or linear function of position; and randomly, according to either a parabolic (mean $\langle\Omega\rangle=5$, spread $\Delta=1$) or Gaussian (mean $\langle\Omega\rangle=5$, standard deviation $\sigma_\Omega=1$) pdf. The scaling exponent for both nonrandom cases is clearly 1, but for the random cases it is between 0.5 and 0.6.

(26) with $i_{ch,j}$ replaced by $\langle i_{ch}\rangle$], where we define $\alpha_{\text{eff}} \equiv \alpha/\langle i_{ch}\rangle$. The array consisted of 50 rotators and a random distribution of bare angular frequencies Ω_j [see Eq. (8)] with average $\langle\Omega\rangle=5$ and spread $\Delta\Omega=0.5$. (Note that assigning the bare oscillator frequencies Ω_j in the LKM is tantamount to assigning junction critical currents in the RSJ model.) We have also calculated α_c via Eq. (30) for the case of a Gaussian pdf with the same average $\langle\Omega\rangle=5$ and standard deviation, $\sigma_\Omega=0.5$. The tails of the Gaussian pdf result in a larger spread in bare frequencies than with the parabolic pdf, which in turn results in a considerably larger value of α_c. For both cases, however, the value of α_c calculated from Eq. (30) agrees well with the numerical solutions of the LKM, at least for $N=50$ and based on a visual inspection of σ_ω versus α.

With Eq. (30) it is easy to determine the scaling relationship between α_c and array size N for large N and for various distributions of bare frequencies. That is, we wish to find the value of the exponent d in the expression $\alpha_c \propto N^d$. Figure 7, which is a log-log plot of α_c versus N for $N \geqslant 50$, shows values of d for four different methods of assigning the bare frequencies: nonrandomly, while following either a parabolic or linear function of position; and randomly, according to either a parabolic or Gaussian pdf. For both types of *nonrandomly* assigned frequencies we find $d=1$; the critical coupling grows linearly with array size. For the *randomly* assigned frequencies we find $d=0.58\pm0.02$ for the parabolic case and $d=0.54\pm0.01$ for the Gaussian case. Note that for both types of random frequencies, the values for α_c are an average over 100 different realizations of frequencies. The error bars on α_c represent the standard deviation of the mean. We note that the two randomly distributed systems exhibit exponents that are approximately equal to 0.5, so that α_c grows *less* rapidly with array size for randomly assigned bare frequencies than for either of the nonrandomly assigned cases. In fact, inspection of Fig. 7 shows that the case of assigning frequencies according to a linear function of position results in the largest value of α_c for a given N of all four cases considered.

Previous work by Liu and co-workers [8] based on a numerical solution of Eq. (26) led to a value of the scaling exponent of $d=2$ for the case of random Gaussian bare frequencies. We suspect the difference with our result (we find $d=0.54$) is due to the technique in determining α_c. If the authors of Ref. [8] used a threshold test to determine α_c, then they would find the smallest value of α for which $\sigma_\omega < C_{\text{threshold}}$, where $C_{\text{threshold}}$ is arbitrary but small. We have found that for increasing N, numerical solutions for σ_ω from the LKM develop long tails in α so that the value of α necessary to satisfy $\sigma_\omega < C_{\text{threshold}}$ can be a sensitive function of the choice of $C_{\text{threshold}}$. Indeed, we have found from numerical experiments with the RSJ model (using double precision variables) that if $C_{\text{threshold}}=10^{-3}$, then $d\approx0.5$, while if $C_{\text{threshold}}=10^{-4}$, then $d\approx2$. This points to the fact that the scaling behavior of α_c with N in the LKM is dependent on the method of analysis. It is interesting, then, that the analytic solution for α_c, obtained from Eq. (30) for the case of Gaussian random frequencies, yields an exponent that is much closer to 1/2 than it is to 2 [25].

Linear Stability analysis of frequency-synchronized state. We can calculate the degree of stability of the fully frequency-synchronized state of the LKM, for $\alpha > \alpha_c$, via a Floquet analysis. Analytic values of the Floquet exponents, λ, for the solutions of Eq. (26) are obtainable for both periodic and open boundary conditions. Loosely speaking, we can think of the values of λ as characterizing the rate at which perturbations to a frequency synchronized state decay. Negative values of λ denote stable synchronization. We find, for periodic and open boundary conditions, respectively,

$$Re(\lambda_m^{\text{periodic}} t_c) = -\frac{2\alpha}{\langle i_{ch}\rangle}\sin^2\left(\frac{\pi m}{N}\right) \quad 0 \leqslant m \leqslant N-1, \tag{31}$$

$$Re(\lambda_m^{\text{open}} t_c) = -\frac{2\alpha}{\langle i_{ch}\rangle}\sin^2\left(\frac{\pi m}{2N}\right) \quad 0 \leqslant m \leqslant N-1, \tag{32}$$

where $t_c \equiv \hbar/(2e\langle I_{ch}\rangle\langle R_h\rangle)$ is the characteristic time scale. Note that above α_c the Floquet exponents grow proportional to α, i.e., the frequency-synchronized state becomes more stable as the coupling α is increased.

V. THERMAL EFFECTS ON SYNCHRONIZATION

In this section we include the effects of an additional thermal noise current in the RSJ model and look specifically at this new current's effect on FS and PS. Keeping with the spirit of previous sections of this paper, we also investigate the synchronization behavior of the LKM with an additional random noise term and compare the dependence of σ_ω on α

for the two models. We find quantitative agreement between the two models over a limited range of temperatures and qualitative agreement over an ever wider range of temperatures.

To include the effects of thermal noise in the junction's resistance, we add a white noise term $I_{N,j}(t)$ to the jth junction in the RSJ model. Note that *every* junction in the ladder experiences such a term. The stochastic currents have the following statistical properties [26]:

$$\langle I_{N,j}(t)\rangle = 0$$

and

$$\langle I_{N,j}(t) I_{N,k}(t+\Delta t)\rangle = \frac{2k_B T}{R_j}\delta_{j,k}\delta(\Delta t),$$

where the angular brackets about stochastic quantities denote an ensemble average, k_B is Boltzmann's constant, T is the absolute temperature, and R_j is the resistance of the jth junction. For simplicity, we will replace R_j by $\langle R_h\rangle$, the average resistance of the horizontal junctions. This should be reasonable for moderate to small amounts of disorder. Expressed in our system of dimensionless units, these relationships take the form

$$\langle i_{N,j}(\tau)\rangle = 0 \quad \text{and} \quad \langle i_{N,j}(\tau) i_{N,k}(\tau+\Delta\tau)\rangle = 4T^*\delta_{j,k}\delta(\Delta\tau), \tag{33}$$

where $i_{N,j} \equiv I_{N,j}/\langle I_{ch}\rangle$ and the dimensionless temperature is $T^* \equiv e k_B T/\hbar\langle I_{ch}\rangle$. We also remind the reader that $\tau \equiv t/(\hbar/2e\langle I_{ch}\rangle\langle R_h\rangle)$.

We generate the $i_{N,j}(\tau)$ for each junction at each time step according to a Gaussian pdf of mean zero and variance $\sigma_T^2 = 4T^*/\Delta\tau$, where $\Delta\tau = 0.01$ is the size of the time step in our fourth-order Runge-Kutta algorithm [27]. It is then possible to vary T^* and observe the effect upon $\sigma_\omega(\alpha)$ and $\langle|r(\alpha)|\rangle_\tau$. For example, Fig. 8 shows that for $N=5$ and open boundary conditions increasing temperature in the RSJ model (solid symbols in the figure) has an adverse effect on frequency synchronization, in that α_c is an increasing function of T^*. We should note that all the results shown in Fig. 8 represent an ensemble average over ten independent runs. Error bars, when visible, represent the standard deviation of the mean of the ten runs. Note that σ_ω develops a long tail as T^* is increased, a fact which makes determining a value of α_c subtle (see Sec. IV). Figure 8 also shows our results for σ_ω for the LKM in the presence of a noise term. Specifically, we modify Eq. (26) to include a white-noise term,

$$\frac{d\theta_j}{d\tau} = \Omega_j + \left(\frac{\alpha}{i_{ch,j}}\right)\sum_{\delta=\pm 1}\sin\left(\frac{\theta_{j+\delta}-\theta_j}{2}\right) + D_N\xi_j(\tau), \tag{34}$$

where $\xi_j(\tau)$ has the same statistical properties as the $i_{N,j}(\tau)$ [see Eq. (33)]. The value for the parameter D_N is chosen as follows. Using a threshold test, we define α_c as the minimum value of the coupling for which $\sigma_\omega < C_{\text{threshold}}$, where we choose $C_{\text{threshold}} = 10^{-3}$. We then pick a single temperature and adjust the value of D_N such that the resulting α_c's from

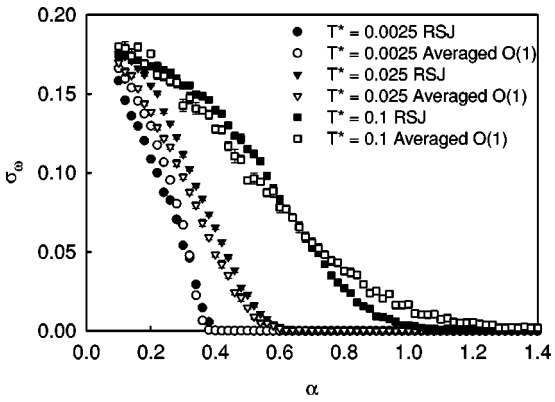

FIG. 8. A comparison of frequency synchronization behavior for the LKM [Eq. (34)] and RSJ model [Eq. (6)] including the effects of thermal noise for three different temperatures $T^* = 0.0025$, 0.025, and 0.1. The array size was $N=5$ with open boundary conditions and $i_B = 5$. We considered one set of random critical currents [Eq. (8)] with a spread of $\Delta = 0.1$. The values of σ_ω represent an ensemble average over ten independent runs to account for the random thermal noise. Note that the agreement between the models is good, except for larger α at higher temperature.

Eq. (34) and the RSJ equations agree to within some specified precision. The value of D_N was then *held fixed* for all other values of T^* and α that were sampled. For example, in Fig. 8 we set $D_N = 1.57$ in order to obtain agreement in the values of α_c from the LKM and RSJ models at a temperature of $T^* = 0.025$. (This temperature was chosen because we typically found it to be roughly in the middle of the range of temperatures we sampled.) The value of D_N was then held fixed in Eq. (34) for the two other sets of temperatures shown in the figure. We note that the general agreement between the RSJ model and the LKM is good, demonstrating again the ability of the LKM to describe the synchronization properties of the overdamped ladder. Not surprisingly, as the temperature is increased sufficiently, the two models show a larger disagreement (see the results for $T^* = 0.1$ in Fig. 8). Presumably this is due to the increased thermal currents in the vertical junctions of the ladder, which are not fully accounted for in the LKM. Note, however, that even at the ''higher'' temperature of $T^* = 0.1$ the two models show qualitative agreement.

In concluding this section, we mention that it would be interesting to look for evidence of stochastic resonance (SR) in the disordered ladder. SR has already been observed in simulations of the fully frustrated ladder ($f = 1/2$) in the presence of a sinusoidal ac bias current [28]. But recently, it has been argued that SR should occur in overdamped systems of coupled oscillators with a constant driving force and white noise [29], conditions that suit nicely our ladder in the presence of thermal noise. Investigation in this area is planned.

VI. UNDERDAMPED LADDERS

In this section we report some preliminary results based on including the effects of junction capacitance on synchronization at zero temperature. We assume the ratio of the junc-

tion critical current to its capacitance is uniform throughout the array and that only the horizontal junctions are disordered. This means that

$$\frac{I_{ch,j}}{C_{h,j}} = \frac{\langle I_{ch}\rangle}{\langle C_h\rangle} = \frac{I_{cv}}{C_v},$$

where $C_{h,j}$ is the capacitance of the jth horizontal junction, and $\langle C_h\rangle$ is the arithmetic mean capacitance. I_{cv} and C_v are the critical current and capacitance, respectively, of the vertical junctions. With the coupling parameter α still defined as in Eq. (5), we arrive at the following set of dimensionless RCSJ equations for left and right nodes, respectively:

$$i_B - i_{ch,j}\sin\phi_j - i_{ch,j}\frac{d\phi_j}{d\tau} - i_{ch,j}\beta_c\frac{d^2\phi_j}{d\tau^2} - \alpha\sin\psi_{l,j}$$

$$-\alpha\frac{d\psi_{l,j}}{d\tau} - \alpha\beta_c\frac{d^2\psi_{l,j}}{d\tau^2} + \alpha\sin\psi_{l,j-1} + \alpha\frac{d\psi_{l,j-1}}{d\tau}$$

$$+\alpha\beta_c\frac{d^2\psi_{l,j-1}}{d\tau^2} = 0, \quad 1 \leqslant j \leqslant N, \tag{35a}$$

$$-i_B + i_{ch,j}\sin\phi_j + i_{ch,j}\frac{d\phi_j}{d\tau} + i_{ch,j}\beta_c\frac{d^2\phi_j}{d\tau^2} - \alpha\sin\psi_{r,j}$$

$$-\alpha\frac{d\psi_{r,j}}{d\tau} - \alpha\beta_c\frac{d^2\psi_{r,j}}{d\tau^2} + \alpha\sin\psi_{r,j-1} + \alpha\frac{d\psi_{r,j-1}}{d\tau}$$

$$+\alpha\beta_c\frac{d^2\psi_{r,j-1}}{d\tau^2} = 0, \quad 1 \leqslant j \leqslant N, \tag{35b}$$

where

$$\beta_c \equiv \frac{2e\langle R_h\rangle^2\langle I_h\rangle\langle C_h\rangle}{\hbar} \tag{36}$$

is a measure of the average junction capacitance in the array. All other quantities in Eq. (35) are defined the same as in Eq. (6).

Equation (35) is combined with Eq. (7) and solved numerically for σ_ω as a function of α for various values of β_c. Figure 9 shows our results for $N=15$, $i_B=5$, and periodic boundary conditions. The critical currents of the horizontal junctions were assigned nonrandomly with a spread of $\Delta = 0.05$. The most interesting behavior appears for $\beta_c \gtrsim 10$, in which we observe a discontinuity in σ_ω at the critical coupling α_c. Recall that for the overdamped ladder the synchronization phase transition was a continuous function of α. Remnants of the $\beta_c \to 0$ behavior are also observed in Fig. 9, since only for sufficiently large capacitance does the transition become discontinuous. In the language of clustering, such as depicted in Fig. 3 for the *overdamped* ladder, this means that the sufficiently underdamped array jumps discontinuously from a single cluster with a common average voltage for α just above α_c, to two clusters characterized by distinct average voltages for α just below α_c.

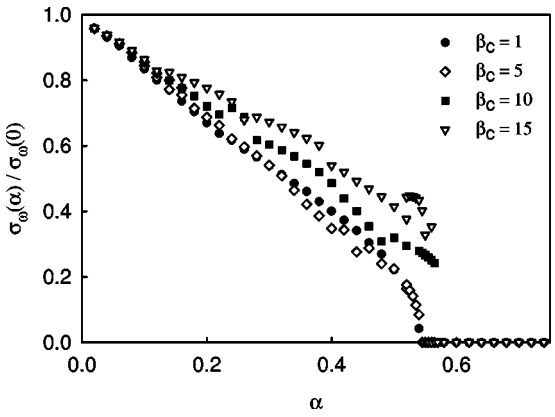

FIG. 9. Frequency synchronization in the underdamped ladder as described by the RCSJ model, Eqs. (35), with $N=15$, $i_B=5$, and periodic boundary conditions. The critical currents of the horizontal junctions were assigned nonrandomly with a spread of $\Delta=0.05$. Note that for $\beta_c \gtrsim 10$ the frequency synchronization transition is discontinuous. This behavior is clearly a result of the junction capacitance, for the transition becomes continuous again as β_c is reduced.

To use the mechanical analogy of an underdamped, driven set of coupled pendula, the effect we are describing corresponds to all the pendula whirling with the same average angular velocity $\langle\omega\rangle$ for $\alpha > \alpha_c$. As the coupling strength is slowly lowered, the array suddenly splits into two sets of pendula, where the elements of a particular set rotate with the same average angular velocity, but the velocities of the two sets themselves have not smoothly evolved from the value $\langle\omega\rangle$. This effect does not appear unless the inertia of a pendulum is sufficiently large compared to the viscous damping it experiences.

A first order, or discontinuous, transition has been observed in studies of the underdamped, *globally* coupled Kuramoto model [30,31]. In that study the authors focused on the phase synchronization order parameter $\langle|r|\rangle$ and using the all-to-all nature of the coupling showed analytically that one would expect a discontinuous transition for sufficient underdamping. We conjecture that our ladder array, upon averaging, would be described by an underdamped *locally* coupled Kuramoto model

$$\beta_c\frac{d^2\theta_j}{d\tau^2} + \frac{d\theta_j}{d\tau} = \Omega_j + \frac{\alpha}{i_{ch,j}}\sum_{\delta=\pm 1}\sin\left(\frac{\theta_{j+\delta}-\theta_j}{2}\right), \tag{37}$$

but it is not clear *a priori* what analytical progress can be made in studying the nature of any discontinuous transition which may be described by Eq. (37) for sufficiently large β_c. Numerical work in comparing the synchronization behavior of Eq. (37) to that of the RCSJ model for the ladder could, however, prove informative. Further work is necessary first to show that Eq. (37) does indeed represent the slow-time dynamics of Eqs. (35).

VII. CONCLUSION

The main result of this paper has been the mapping from the RSJ model for the overdamped Josephson ladder to the

locally coupled Kuramoto model [Eq. (26)]. We argued that if one is interested in the frequency and phase synchronization behavior of a ladder array with critical current and resistive disorder among the horizontal junctions, then one need mainly be concerned with the slow time-scale dynamics, as opposed to the fast time-scale dynamics, of the junctions. When the fast dynamics, set by the time scale at which the junction voltages oscillate, is integrated out of the RSJ equations the result is the locally coupled Kuramoto model (LKM). As a check that the LKM does indeed describe the synchronization behavior of the RSJ model, we compared the spread of average voltages along the ladder, σ_ω, which gives information about the degree of frequency synchronization of the junctions, and the Kuramoto order parameter $\langle|r|\rangle$, which measures the degree of phase synchronization, for the two models over a broad range of array sizes, bias currents, critical currents, and for both periodic and open boundary conditions. We found that for sufficiently high bias currents, $i_B \gtrsim 3$, and for critical current disorders of up to 10% the two benchmark quantities σ_ω and $\langle|r|\rangle$ agree quite well for the two models. We also argued that the restriction to high bias currents was required to prevent phase slips in the vertical junctions of a plaquette that would not be accounted for in the LKM. Inclusion of junction capacitance, $\beta_c \neq 0$, is a nontrivial modification to the system. Preliminary results for such an underdamped ladder show that σ_ω exhibits a discontinuous transition as a function of the junction coupling strength α when the junction capacitance is sufficiently large (i.e., $\beta_c > \beta_c^*$ where β_c^* is a function of array size, bias current, etc.). For a small but finite amount of capacitance, $0 < \beta_c \leqslant \beta_c^*$, the frequency synchronization transition is a continuous function of α.

Future work on synchronization studies in disordered Josephson ladders could include looking for stochastic resonance in the dc-driven overdamped array when the bias current is less than the junction critical currents, as well as looking for noise-induced resonance effects in the underdamped ladder when biased in the voltage state [32]. Finally, considerable work remains in understanding the connection between the RCSJ equations for the underdamped ladder and the underdamped LKM [Eq. (37)].

ACKNOWLEDGMENTS

This project was supported by the Ohio Wesleyan University Summer Research Program which was funded in part by the McGregor Fund.

[1] A.T. Winfree, *The Geometry of Biological Time* (Springer-Verlag, New York, 1980).
[2] Y. Kuramoto, *Chemical Oscillations, Waves and Turbulence* (Springer-Verlag, Berlin, 1984).
[3] A. Pikovsky, M. Rosenblum, and J. Kurths, *Synchronization: A Universal Concept in Nonlinear Sciences* (Cambridge University Press, Cambridge, 2001).
[4] A.T. Winfree, J. Theor. Biol. **16**, 15 (1967).
[5] Y. Kuramoto, in *International Symposium on Mathematical Problems in Theoretical Physics*, edited by H. Araki, Lecture Notes in Physics, Vol. 39 (Springer, New York, 1975). See also Ref. [2].
[6] For a historical and mathematical review of basic aspects of the GKM, see S.H. Strogatz, Physica D **143**, 1 (2000).
[7] S.H. Strogatz and R.E. Mirollo, Physica D **31**, 143 (1988).
[8] Z. Liu, Y.-C. Lai, and F.C. Hoppensteadt, Phys. Rev. E **63**, 055201 (2001).
[9] Z. Zheng, G. Hu, and B. Hu, Phys. Rev. Lett. **81**, 5318 (1998).
[10] S. Shinomoto and Y. Kuramoto, Prog. Theor. Phys. **75**, 1319 (1986).
[11] R.S. Newrock, C.J. Lobb, U. Geigenmüller, and M. Octavio, *Solid State Physics* (Academic Press, San Diego, 2000), Vol. 54.
[12] B. Vasilić, P. Barbara, S.V. Shitov, and C.J. Lobb, Phys. Rev. B **65**, 180503 (2002).
[13] G. Filatrella, B. Straughn, and P. Barbara, J. Appl. Phys. **90**, 5675 (2001).
[14] M. Darula, T. Doderer, and S. Beuven, Supercond. Sci. Technol. **12**, R1 (1999).
[15] M.V. Fistul and J.B. Page, Phys. Rev. E **64**, 036609 (2001); E. Trías, J.J. Mazo, and T.P. Orlando, Phys. Rev. Lett. **84**, 741 (2000); P. Binder, D. Abraimov, A.V. Ustinov, S. Flach, and Y. Zolotaryuk, *ibid.* **84**, 745 (2000).
[16] For example, see B.R. Trees, in *Studies of High Temperature Superconductors* (NOVA Science Publishers, New York, 2001), Vol. 39.
[17] K. Wiesenfeld, P. Colet, and S.H. Strogatz, Phys. Rev. Lett. **76**, 404 (1996).
[18] K. Wiesenfeld, P. Colet, and S.H. Strogatz, Phys. Rev. E **57**, 1563 (1998).
[19] H.-A. Tanaka, A.J. Lichtenberg, and S. Oishi, Phys. Rev. Lett. **78**, 2104 (1997); Physica D **100**, 279 (1997).
[20] The I_cR product has been found to be quite uniform in arrays of SNS junctions. See S.P. Benz, Appl. Phys. Lett. **67**, 2714 (1995).
[21] Actually, Eqs. (6) and (7) result in $3N-1$ equations in $3N-2$ unknowns. We therefore do not apply Eq. (6b) to the lower right node (chosen arbitrarily). A similar effect arises in the solution of the RSJ equations for the superconducting phases at the $2N$ *nodes* of the array. In that case, one must arbitrarily set the phase at one of the nodes to zero, i.e., ground a node.
[22] G. Filatrella and K. Wiesenfeld, J. Appl. Phys. **78**, 1878 (1995).
[23] See Refs. [17] and [18] as well as: J.W. Swift, S.H. Strogatz, and K. Wiesenfeld, Physica D **55**, 239 (1992); K. Wiesenfeld and J.W. Swift, Phys. Rev. E **51**, 1020 (1995).
[24] See Ref. [7] or also A.H. Cohen, P.J. Holmes, and R.H. Rand, J. Math. Biol. **13**, 345 (1982).
[25] We should note that we find it necessary to use a threshold test to determine α_c when solving the RSJ equations numerically.
[26] A. Barone and G. Paternó, *Physics and Applications of the*

Josephson Effect (Wiley, New York, 1982).
[27] C.D. Tesche and J. Clarke, J. Low Temp. Phys. **29**, 301 (1977).
[28] B.J. Kim, M.-S. Choi, P. Minnhagen, G.S. Jeon, H.J. Kim, and M.Y. Choi, Phys. Rev. B **63**, 104506 (2001).
[29] M. Qian and X.J. Zhang, Phys. Rev. E **65**, 031110 (2002).
[30] H.-A. Tanaka, A.J. Lichtenberg, and S. Oishi, Phys. Rev. Lett. **78**, 2104 (1997).
[31] H.-A. Tanaka, A.J. Lichtenberg, and S. Oishi, Physica D **100**, 279 (1997).
[32] H. Hong and M.Y. Choi, Phys. Rev. E **62**, 6462 (2000).